Identification of Grid Impedance During Severe Faults

Betz, Robert; Taul, Mads Graungaard

Published in:
2019 IEEE Energy Conversion Congress and Exposition, ECCE 2019

DOI (link to publication from Publisher):
10.1109/ECCE.2019.8911873

Publication date:
2019

Document Version
Accepted author manuscript, peer reviewed version

Identification of Grid Impedance During Severe Faults

Robert Eric Betz
School of Electrical Engineering and Computing
University of Newcastle
Newcastle, Australia
robert.betz@newcastle.edu.au

Mads Graungaard Taul
Dept. of Energy Technology
Aalborg University
Aalborg, Denmark
mkg@et.aau.dk

***Abstract*—Grid-connected converters, when subject to grid fault conditions, should stay connected and support the network voltage via reactive power injection. The fulfilment of this requirement strongly depends on the dynamics and stability of the converter control system. It can be shown that local static instability, and the consequent local dynamic instability can be avoided if the grid impedance during the fault is known. This paper proposes a novel method to identify the grid impedance during the fault by using the grid fault disturbance as an identification pulse. The proposed identification method is implemented in a proof-of-concept detailed simulation model, and verified with experimental results.**

NOMENCLATURE

$\mathbf{Z}$	The line impedance ($= R + jX_L$).
ω	Frame angular velocity.
ω_c	The current control reference frame angular velocity.
ω_I	Angular velocity of current space phasor relative to ω.
ω_{syn}	Synchronous frame angular velocity.
$\hat{\mathbf{X}}$	The magnitude of generic phasor $\vec{\mathbf{X}}$.
$\vec{\mathbf{I}}_{\mathrm{WP}}$	Wind Park injected current phasor.
$\vec{\mathbf{V}}_{\mathrm{G}}$	Grid voltage phasor.
$\vec{\mathbf{V}}_{\mathrm{WP}}$	Wind Park connection voltage phasor.
$\lvert\underline{x}\rvert$	Space vector magnitude of $\underline{x}$.
$\underline{i}_r$	Wind Park rotating frame grid current space vector.
$\underline{i}_{WP}$	Wind Park stationary frame grid current space vector.
$\underline{v}_{Gr}$	Rotating frame grid voltage space vector.
$\underline{v}_G$	Stationary frame grid voltage space vector.
$\underline{v}_r$	Wind Park rotating frame voltage space vector.
$\underline{v}_{WP}$	Wind Park stationary frame voltage space vector.
φ_I	Grid current phasor angle.
φ_Z	Line impedance angle $= \tan^{-1}\frac{X_L}{R}$.
I_a	Real (active) component of the phasor grid current.
I_R	Reactive component of the phasor grid current transformed to $-\varphi_Z$ axis.
I_r	Reactive component of the phasor grid current.
L	Line inductance.
R	Line resistance.
$x_{d,qr}$	d or q component of generic space vector x in a rotating reference frame.
PLL	Phase Locked Loop.
PR	Proportional Resonant.
SRF-PLL	Synchronous Reference Frame PLL.
WP	Wind Park.

I. INTRODUCTION

The majority of renewables are interfaced to the grid using a grid-following current-controlled converter. Under normal operating conditions these converters would be feeding maximum power into the grid – i.e. the injected current is in-phase, or near in-phase with the voltage at the converter grid connection point. The current injection level is determined by the power available, the power commands, and the grid impedance at the connection point such that the connection is statically stable.

However, under fault conditions (and also weak grid conditions), there is a risk of the converter grid connection becoming statically unstable. This static instability can also lead to dynamic instability via a feedback process through the Phase-Locked Loop (PLL) in the converter control system [1]–[5].

In order to understand why knowledge of the grid impedance can assist with maintaining stability at the converter connection, a brief review of how static instability occurs will be presented. Consider Fig. 1, which is an approximate equivalent circuit of a Wind Park (WP) (or a Solar Park) connected to the grid through a complex line impedance of $\mathbf{Z}[\Omega]$. It is assumed that the WP can be aggregated together and represented by a single converter system interface.

Applying KVL in steady state phasor form to Fig. 1, one can write

$$\vec{\mathbf{V}}_{\mathrm{G}} = \hat{\mathbf{V}}_{\mathrm{WP}} - \vec{\mathbf{I}}_{\mathrm{WP}}\mathbf{Z} \tag{1}$$

assuming that the $\vec{\mathbf{V}}_{\mathrm{WP}}$ phasor is the reference phasor. For the sake of this explanation assume that $\vec{\mathbf{I}}_{\mathrm{WP}} = \hat{\mathbf{I}}_{\mathrm{WP}}e^{-j\pi/2}$ – i.e. the WP is injecting purely reactive current to support the grid. This is the situation required by most grid codes when a fault occurs. Furthermore, assume that $\mathbf{Z} = \hat{\mathbf{Z}}e^{j\pi/4}$ – i.e. the line impedance has an X/R ratio of 1. The grid voltage magnitude, $\hat{\mathbf{V}}_{\mathrm{G}}$, and its frequency are *assumed to be constant*. The solution to (1) is shown graphically in Fig. 2 for different magnitudes of injected current. Note that the magnitude of $\vec{\mathbf{V}}_{\mathrm{G}}$ is fixed and the angle of the injected current is fixed, which means that the magnitude of $\vec{\mathbf{V}}_{\mathrm{WP}}$ has to change to allow (1) to be satisfied. As $\hat{\mathbf{I}}_{\mathrm{WP}}$ increases (through points 1, 2 and 3), the $\angle\vec{\mathbf{V}}_{\mathrm{G}}$ changes with respect to the $\vec{\mathbf{V}}_{\mathrm{WP}}$ reference. If $\hat{\mathbf{I}}_{\mathrm{WP}}$ is increased at Point 3 there can be no solution to the equations if the frequency remains the same. A constant

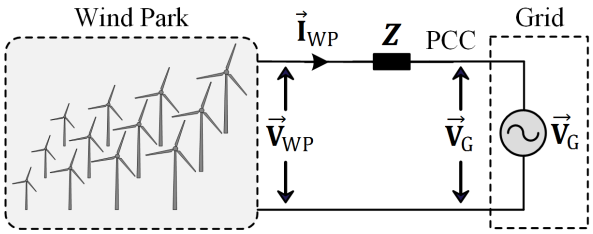

Fig. 1: Single line diagram of a Wind Park connected to the grid.

frequency solution means that the resultant $\vec{\mathbf{V}}_{\mathrm{G}}$ vector either has to increase in magnitude, or the angle of the current has to change, both of which violate the initial assumptions. This is the point of static instability. Note that Point 4 is still a statically unstable solution even if the angle of the current vector is allowed to change.

If there is a fault that results to $\hat{\mathbf{V}}_{\mathrm{G}}$ collapsing to a small value, and if $\hat{\mathbf{I}}_{\mathrm{WP}}$ remains unchanged, then one can see that $\angle\vec{\mathbf{V}}_{\mathrm{G}} - \angle\vec{\mathbf{V}}_{\mathrm{WP}}$ can easily be greater than $90°$. Therefore, instability can be triggered by a collapse in $\hat{\mathbf{V}}_{\mathrm{G}}$, increases in $\hat{\mathbf{I}}_{\mathrm{WP}}$, changes to $\angle\vec{\mathbf{I}}_{\mathrm{WP}}$, and high grid impedances (i.e. very weak connections).

The frequency changes in the converter grid voltage $\vec{\mathbf{V}}_{\mathrm{WP}}$ associated with the onset of instability cause the control system PLLs to shift their frequency, which in-turn feeds back into the control. This feedback loop is one of the primary reasons for the loss of synchronisation of the inverter control system. Considerable research has been undertaken to understand the dynamics of, and to try and alleviate this loss of synchronism after static instability occurs [1]–[3], [6]. However, it can be logically concluded that if static instability is avoided then such synchronisation issues will not occur.

It is well known [7] that the critical static instability injected current when $\angle\vec{\mathbf{I}}_{\mathrm{WP}} = -\pi/2$ rad is

$$\hat{\mathbf{I}}_{\mathrm{WP}} = \frac{\hat{\mathbf{V}}_{\mathrm{G}}}{R}. \tag{2}$$

Therefore if $\hat{\mathbf{I}}_{\mathrm{WP}} > \frac{\hat{\mathbf{V}}_{\mathrm{G}}}{R}$ then the system will be statically unstable. To know this limit, obviously one needs to know the grid voltage and the line resistance R. It can be shown that the current limit for the more general case is [7]

$$I_{R_{\max}} = \frac{\hat{\mathbf{V}}_{\mathrm{G}}}{\hat{\mathbf{Z}}} \tag{3}$$

where $I_R = I_r \cos\varphi_Z - I_a \sin\varphi_Z$ and

$I_a \triangleq$ the active or real current

$I_r \triangleq$ the reactive or imaginary current

$\varphi_Z \triangleq$ the line impedance angle $= \arctan\dfrac{X_L}{R}$

Remark 1. Equation (3) indicates that the limit for instability is again dependent on the magnitude of the grid voltage and the line impedance. ■

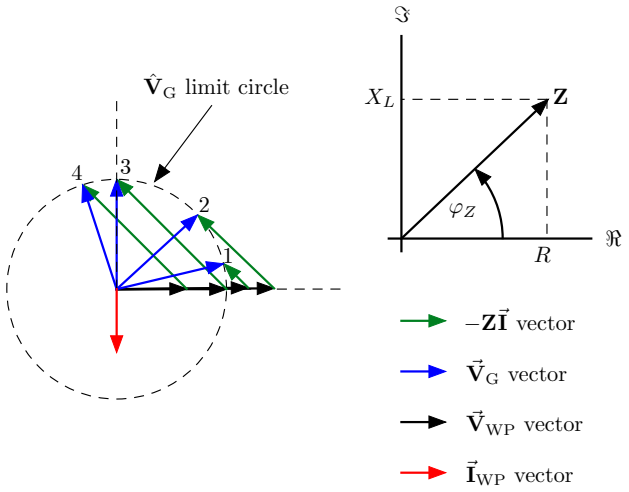

Fig. 2: Vector diagram for the WP connection case describing the static stability and instability.

Remark 2. In (3) if $\hat{\mathbf{V}}_{\mathrm{G}} = 0$ then the current level where the system is statically unstable is zero Amps. However, it can be shown that if $\varphi_I = -\varphi_Z$ there is no limit to the injected current magnitude. This condition means that $\frac{I_r}{I_a} = -\frac{X_L}{R}$. So even under this condition, knowledge of $\mathbf{Z}$ is important in order to ensure stability. ■

Remark 3. $\hat{\mathbf{V}}_{\mathrm{G}}$ is an unknown quantity in both (2) and (3). However, if $\mathbf{Z}$ is known then this together with the injected current and the connection point voltage allows $\vec{\mathbf{V}}_{\mathrm{G}}$ to be determined. ■

We have now established that knowledge of $\mathbf{Z}$ is essential for calculating the value of injected currents to avoid instability. The expressions apply generally, under both normal operation as well as fault conditions.

In general the grid impedance during a fault will be different to the impedance before the fault and post fault. Furthermore, the grid codes require a response within 10 to 20 msec, which means that the grid impedance has to be identified within this period so that an appropriate control to simultaneously satisfy the grid codes, and ensure connection point stability, can be applied.

In the next section a new technique to identify the line impedance during the fault condition will be developed. The fault type being considered in this paper is a three phase fault, since single phase faults often don't create a severe enough dip in the positive sequence component of the grid voltage to cause static instability.

II. The Method

There are a multitude of techniques in the literature for determining grid impedance (some of which are [8]–[11]). Many of these methods involve sophisticated signal processing techniques designed to accurately determine slowly varying grid impedances under normal operation, and are not suitable for rapidly estimating the grid impedance when a fault occurs.

The technique developed below is loosely based on the two point method [8]. This method is usually implemented under steady-state conditions. From (1) we can write

$$\vec{\mathbf{I}}_{\mathrm{WP}} = \frac{\vec{\mathbf{V}}_{\mathrm{WP}} - \vec{\mathbf{V}}_{\mathrm{G}}}{\mathbf{Z}}. \tag{4}$$

If two time separated samples of both the $\vec{\mathbf{I}}_{\mathrm{WP}}$ and $\vec{\mathbf{V}}_{\mathrm{WP}}$ phasors are taken one can write

$$\vec{\mathbf{I}}_{\mathrm{WP1}}\mathbf{Z} = \vec{\mathbf{V}}_{\mathrm{WP1}} - \vec{\mathbf{V}}_{\mathrm{G}} \tag{5}$$

$$\vec{\mathbf{I}}_{\mathrm{WP2}}\mathbf{Z} = \vec{\mathbf{V}}_{\mathrm{WP2}} - \vec{\mathbf{V}}_{\mathrm{G}} \tag{6}$$

which can be subtracted from each other and rearranged to give

$$\mathbf{Z} = \frac{\vec{\mathbf{V}}_{\mathrm{WP1}} - \vec{\mathbf{V}}_{\mathrm{WP2}}}{\vec{\mathbf{I}}_{\mathrm{WP1}} - \vec{\mathbf{I}}_{\mathrm{WP2}}}. \tag{7}$$

To ensure that $\vec{\mathbf{I}}_{\mathrm{WP1}} - \vec{\mathbf{I}}_{\mathrm{WP2}} \neq 0$, a test pulse is injected between the two sample instants. Clearly there are issues with this technique, namely

- the network has to be substantially perturbed with a test pulse;
- there is a lack of precision with respect to when the system is in steady state after the test pulse injection so that the second sample can be taken;
- the steady state assumption implies that the technique is not suitable for rapid impedance estimation.

The technique does rely on the assumption that the grid voltage does not change for each of the samples, allowing it to be eliminated by the subtraction.

The basic idea behind the method presented in this paper is to use the fault grid voltage step change as the excitation pulse to identify the grid impedance. It does not rely on a user input test pulse and it is required to work under dynamic conditions. By expressing the space-vector equivalent equation in a stationary-reference frame, (1) can be written as

$$\underline{v}_{WP} = L\frac{d\underline{i}_{WP}}{dt} + R\underline{i}_{WP} + \underline{v}_{G}. \tag{8}$$

If this expression is manipulated into a reference frame rotating at an angular velocity of ω rad/sec, it becomes

$$\underline{v}_{r} = R\underline{i}_{r} + L\frac{d\underline{i}_{r}}{dt} + j\omega L\underline{i}_{r} + \underline{v}_{Gr}. \tag{9}$$

Let us consider the $\frac{d\underline{i}_r}{dt}$ term in this equation, which can be written as

$$\begin{aligned} L\frac{d\underline{i}_{r}}{dt} &= L\frac{d}{dt}\left(|\underline{i}_{r}|e^{j\varphi_I}\right) \\ &= L\left(|\underline{i}_{r}|e^{j\varphi_I}j\frac{d\varphi_I}{dt} + e^{j\varphi_I}\frac{d}{dt}|\underline{i}_{r}|\right). \end{aligned} \tag{10}$$

Assuming that the converter current controller can maintain a constant current magnitude over the duration of the sampling period then it is reasonable to consider that $\frac{d}{dt}|\underline{i}_r| = 0$ which allows (9) to be written as

$$\underline{v}_{r} = R\underline{i}_{r} + j(\omega_I + \omega)L\underline{i}_{r} + \underline{v}_{Gr} \tag{11}$$

where ω_I is the angular velocity of the current vector relative to the synchronously rotating frame.

There are a variety of frames that could be chosen for this expression. For example, an obvious reference frame is the current control frame which is aligned with the $\underline{v}_{WP}$ space vector. However, under fault conditions, the $\underline{v}_{WP}$ vector can be rotating at a variable angular velocity. This fact has implications on the $\underline{v}_{Gr}$ samples in this frame – it will have different values between the two samples. Therefore, the grid voltage will not be eliminated by differencing. A constant angular velocity synchronous reference frame with an angular velocity of $\omega = \omega_{syn}$ implies that the samples of the $\underline{v}_{Gr}$ vector will be the same for the two samples (under the previous assumption that the grid voltage is constant during the fault). The key to understanding how the algorithm works is to consider what is happening to the reference frames.

Prior to the fault, the control reference frame is aligned with the $\underline{v}_r$ vector. When the fault occurs, the $\underline{v}_r$ vector effectively jumps to a different position to dynamically satisfy KVL. In the meantime, the current vector is still in the previous position because the PLL that generates the control reference frame is designed to have a bandwidth that prevents rapid following of the voltage vector jump. However, over time, the action of the PLL causes the control reference frame to move towards the voltage vector. This in-turn means that the current vector is moving with respect to the pre-fault ω_{syn} reference frame. The relative angular velocity of the current vector with respect to ω_{syn} is ω_I rad/sec. If the $\underline{v}_r$ is changing angular velocity as well, then this will have different values over time relative to the ω_{syn} reference frame. It is these differences, caused by the fault, that provide the excitation to allow the parameters to be calculated.

Remark 4. Clearly the bandwidth of the current control PLL is an important factor in the operation of the algorithm. If to slow then there will not be enough difference in the samples of the current, and if too high then phase noise will affect the accuracy of the samples.

Another important factor with respect to accuracy is the time between the samples. If the sample interval is small then the inevitable "derivative" noise introduced will be too high. The maximum sample interval time is constrained by the grid code response time. ■

Let ω_c be the angular velocity of the control reference frame pre-fault, which means $\omega_c = \omega_{syn}$ and $\omega_I = \omega_c - \omega_{syn} = 0$. During the fault, the control frame is trying to realign with the new position of $\underline{v}_r$, and therefore $\omega_I = \omega_c - \omega_{syn}$. Consequently, (11) becomes

$$\underline{v}_{r} = R\underline{i}_{r} + j(\omega_c - \omega_{syn} + \omega_{syn})L\underline{i}_{r} + \underline{v}_{Gr} \tag{12}$$

$$\therefore \underline{v}_{r} = R\underline{i}_{r} + j\omega_c L\underline{i}_{r} + \underline{v}_{Gr}. \tag{13}$$

If (13) is expanded into dq form, and two samples of the dq quantities are subtracted (similar to the steady-state form of the two point method), then the following equations can be obtained

$$v_{dr1} - v_{dr2} = R(i_{dr1} - i_{dr2}) + L(\omega_{c2} i_{qr2} - \omega_{c1} i_{qr1}), \quad (14)$$

$$v_{qr1} - v_{qr2} = R(i_{qr1} - i_{qr2}) + L(\omega_{c1} i_{dr1} - \omega_{c2} i_{dr2}) \quad (15)$$

which can be solved simultaneously to give the expressions for R and L as

$$L = \frac{\Delta v_{qr} \Delta i_{dr} - \Delta v_{dr} \Delta i_{qr}}{A - B} \quad (16)$$

$$R = \frac{\Delta v_{dr} - L(\omega_{c2} i_{qr2} - \omega_{c1} i_{qr1})}{\Delta i_{dr}} \quad (17)$$

where

$$1, 2 \triangleq \text{ the sample number}$$
$$\Delta v_{dr} = v_{dr1} - v_{dr2};\ \Delta v_{qr} = v_{qr1} - v_{qr2}$$
$$\Delta i_{dr} = i_{dr1} - i_{dr2};\ \Delta i_{qr} = i_{qr1} - i_{qr2}$$
$$A = \omega_{c1}(i_{dr1} \Delta i_{dr} + i_{qr1} \Delta i_{qr})$$
$$B = \omega_{c2}(i_{dr2} \Delta i_{dr} + i_{qr2} \Delta i_{qr})$$
$$\omega_{c1,2} \triangleq \text{ samples of } \omega_c \text{ (the PLL freq).}$$

III. Simulation Results

A. Ideal Model

As an initial test of the concept, an ideal Modelica SystemModeler® simulation was written. This simulation modeled the inverter as an ideal current source. The parameters used were those for the real wind park case from [3], with $R = 0.00220935\Omega$ and $L = 56.67\mu\text{H}$ which corresponds to $\hat{\mathbf{Z}} = 0.21\text{pu}$ and $X/R = 8$. The sampling interval was 10 msec, the first sample occurred at 1 sec, and the voltage dip was down to 0.0258pu (which is on the edge of static instability). The results of this simulation appear in Figs. 3 and 4. The voltage dip in Fig. 3a is a deep one. Fig. 3b shows the reference and actual currents viewed from the control, voltage and synchronous estimation reference frames. In Fig. 3b the i_d and i_q currents are measured relative to the true (i.e. aligned with the actual voltage vector) reference frame. The i_{dsyn} and i_{qsyn} currents are measured relative to the constant angular velocity synchronous reference frame, and i_d^{ref} and i_q^{ref} are the reference currents relative to the controller reference frame. Fig. 4a shows the change of the frame angles with the onset of the fault. Finally, Fig. 4b shows the parameter estimates. The relative estimation errors are $R_{\text{err}} = 0.06\%$ and $L_{\text{err}} = 0.1\%$. Whilst this is an ideal simulation, and a particularly good case, it nevertheless shows the potential of the technique.

B. Detailed Switching Model

To further verify the proposed impedance identification method, a detailed switching model was developed for the system, implemented in MATLAB's Simulink together with the PLECS Blockset. It uses a two-level, three-phase converter with an output LCL filter to replace the WP shown in Fig. 1. The converter is implemented as a grid-following converter where an SRF-PLL is used to extract the phase information of the voltage at the point of connection, and a PR current regulator is used to track the dq-axes reference currents as shown in Fig. 5. The key parameters of the system are listed in Table I. It should be noted that the per unit quantities of the grid impedance are equivalent to $R = 0.6\Omega, L = 14.3\text{mH}$ which corresponds to $\hat{\mathbf{Z}} = 0.2\text{pu}$ and $X/R = 7.5$. This is similar to the parameters used for the idealised simulation results but implemented for a down-scaled setup which is to be experimentally validated in the following section.

System Parameters	Value
Rated Power	7.35 kVA
Nominal grid voltage (l-l, rms)	400 V
dc-link voltage	730 V
Nominal frequency	50 Hz
Switching/sampling frequency	10 kHz
Converter-side inductor L_1	0.072 pu
Grid-side inductor L_2	0.043 pu
Filter capacitor C_f	0.068 pu
Grid impedance $\boldsymbol{Z}$	0.028 +0.2j pu
Proportional gain of SRF-PLL	101.8
Integral gain of SRF-PLL	5184
Proportional gain of current controller	10
Resonant gain of current controller	1000
Fault and pre-fault current magnitude	1 pu

Table I: Parameters of the network, filter, and control of Figure 5.

A severe fault where the $\hat{\mathbf{V}}_{\text{G}}$ drops to 0.05pu is studied with the grid-tied converter injecting 1pu active current both before and during the fault. This represents a scenario where the converter is operating in the unstable region defined by the static limitations of the network. The simulation result for this case is shown in Fig. 6a where the reference currents, the actual currents relative to the true reference frame, and the injected currents in the orientation of the slowly varying reference frame are shown, all in dq quantities. The identified impedance and the three-phase voltages at the WP connection point appear on the bottom two plots in Fig. 6a. Even with the unstable characteristics of the system when the fault occurs, the identified resistance and inductance are 0.561Ω and 14.38mH, with a relative error of -6.5% and -0.56%, respectively. Since the system is statically unstable during the fault, i.e. the PLL frequency is drifting during the fault, and the d-axis current measured from the synchronous slowly varying PLL (i_{dsyn}) can be seen to increase its operating frequency. This occurs as the synchronous PLL remains at 50 Hz whereas the frequency of the injected current drifts away from 50 Hz, dictated by the frequency of the control PLL.

Performing the same study but with current injection as required by most grid codes (Fig. 6b), the relative identification errors are -1.33% and 2.23% for the resistance and inductance, respectively. Once again, as was seen in Fig. 6a, accurate identification of the line parameters was achieved, even though loss of synchronisation and transient instability

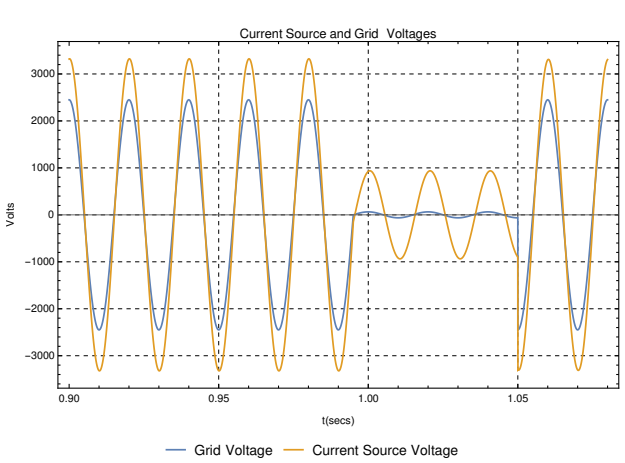

(a) Supply and converter voltages.

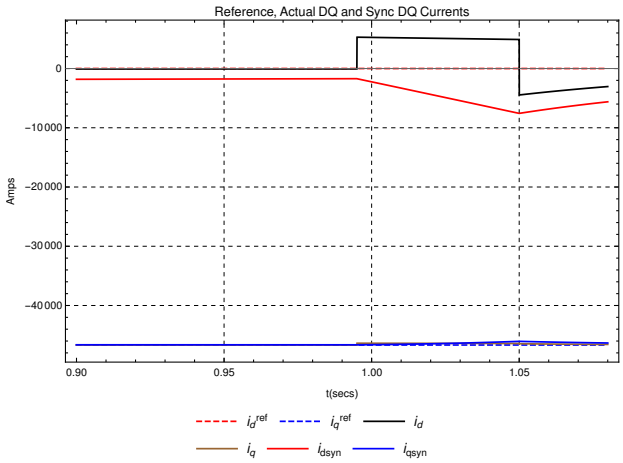

(b) DQ currents.

Fig. 3: Ideal test results

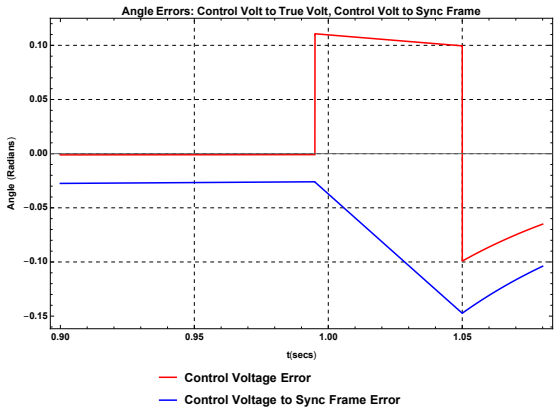

(a) Frame angle variations.

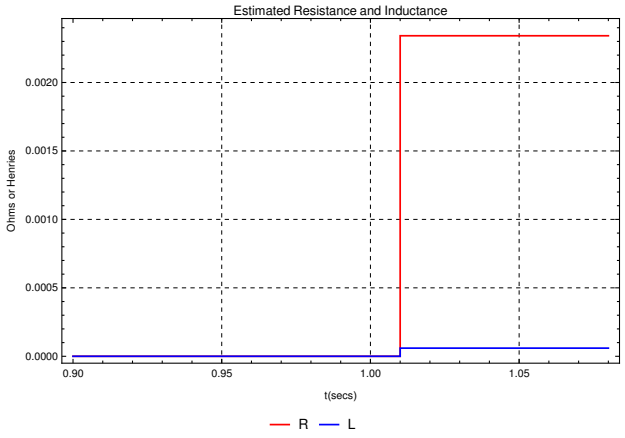

(b) Parameter estimates $\hat{R} = 0.00234143\Omega$ and $\hat{L} = 59.6059\mu$H.

Fig. 4: Ideal simulation results for $i_d = 0$kA and $i_q = -46.67$kA (i.e. $-90°$), Dip $\hat{\mathbf{V}}_{\mathrm{G}} = 0.0258$pu.

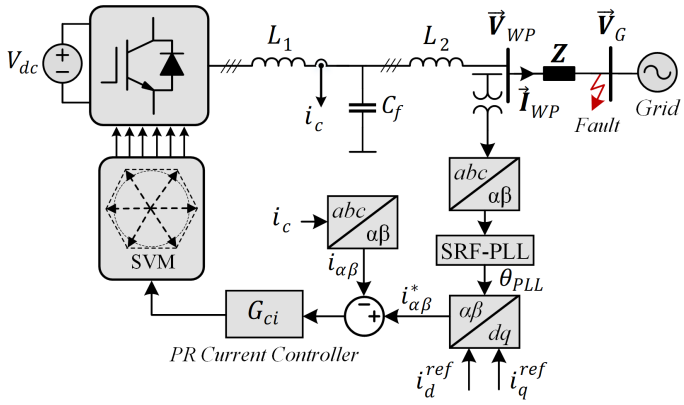

Fig. 5: Detailed view of the converter control, filtering, and structure used for the simulation.

occurs during the fault. For the simulations, the sampling interval was 10 ms and the first sample was taken 10 ms into the fault. When comparing the results from the detailed model with ideal simulation, the waveforms contain much higher order dynamics from parasitic elements not included in the ideal simulation. These result in transients when the grid voltage drops. However, with the slow synchronous PLL, sufficient change in the currents after the transients are enough to establish an accurate estimate.

Accordingly, even when switching harmonics, current controller dynamics and controller delays are included, the proposed method enables reasonable accurate $\mathbf{Z}$ estimates, which can be used in for control strategies during severe faults.

Remark 5. It should be noted that the two case studies presented in Fig. 6 are both statically unstable during the fault. No attempt has been made to alter the control so that the instability is avoided. These simulations show that the

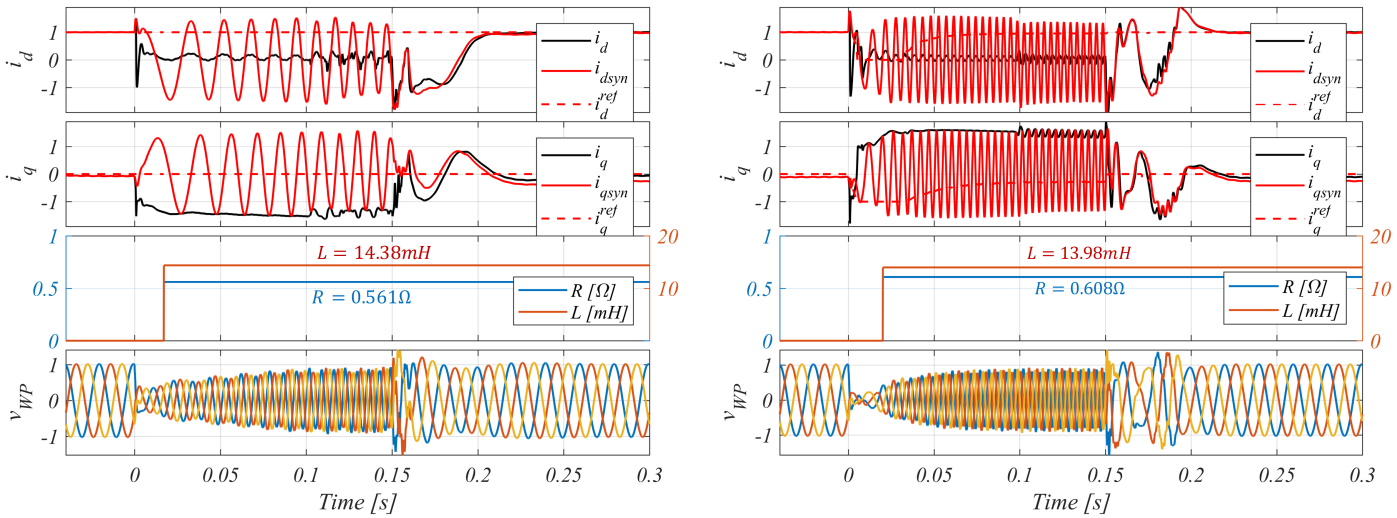

(a) Identification of grid impedance during active current injection. $\hat{R} = 0.561\Omega$ and $\hat{L} = 14.38mH$.

(b) Identification of grid impedance during current injection based on the grid code. $\hat{R} = 0.608\Omega$ and $\hat{L} = 13.98mH$.

Fig. 6: Test results obtained from the detailed simulation model. $\hat{\mathbf{V}}_{\mathrm{G}} = 0.05$ pu during the fault.

identification method is dependent only on the circuit topology, and does not depend static stability assumptions.

Furthermore, as it can be seen from Fig. 6a the system cannot follow its current reference as this together with the network parameters and fault voltage level does not result in the existence of a stable operating point. Therefore, the injected currents will automatically relocate themselves in order to satisfy the network conditions. ■

An attentive reader may observe that i_q is positive in Fig. 6b, which from the passive sign convention indicates that the converter absorbs reactive power which should result in a voltage collapse. However, as it can be seen, the voltage at the WP connection point is actually supported during the fault. This occurs as no limiters are used on the PLL, which during the instability reaches a large negative frequency (usually not allowed in real applications where the PLL frequency is tightly limited). This means that the injected currents are actually negative sequence rather than positive sequence, where positive reactive current will result in a voltage boost as noticed.

To that end, as the converter looses stability during the fault, the converter currents can no longer be controlled to its references, and follow values satisfying the networks KVL equations. This obviously means that in such conditions the assumption that $\frac{d}{dt}|\underline{i}_r| = 0$ can no longer be guaranteed. Therefore, to satisfy this assumption, it may be preferred for the converter to be controlled in a stable manner initially when the identification algorithm is run, where-after the converter operating point can be altered. In this case, the converter current magnitude can be tightly controlled. Nevertheless, as it has been shown, accurate identification is possible even though the assumption that $\frac{d}{dt}|\underline{i}_r| = 0$ is not fully satisfied.

IV. Experimental Results

To further validate the proposed rapid parameter identification method and reveal its sensitivity to measurement errors and noise, the two simulation cases presented in Fig. 6 are experimentally tested in a laboratory setup. A detailed description of the experimental setup is given in [6] and the circuit and controller parameters are listed in Table. I. The experimental results are shown in Fig. 7a for active current injection and in Fig. 7b for current injection based on grid code requirements for dynamic voltage support. The relative errors of the identification for active current injection are 8.00% and 3.17% for the resistance and inductance, respectively. Likewise, for the case in Fig. 7b, the identification resulted in a relative error of -5.17% and 2.80% for the resistance and inductance, respectively. For the identification in Fig. 7a, the sampling interval was 10 ms and the first sample was taken 7 ms into the fault whereas for the identification in Fig. 7b, the sampling interval was 15 ms and the first sample was taken 15 ms into the fault.

It should be mentioned, that the reference values for the resistance and inductance is not fully known in the laboratory as the values of the passive components are difficult to precisely measure. The resistance is the largest source of error as its value was changing with the operating conditions of the converter. Notwithstanding these comments, the identification algorithm appears to give reasonable accuracy, taking into account real world conditions with parameter variations, noise on measurements, control delays, sampling noise, switching noise etc.. It was observed that the identification is rather sensitive to the dynamics of the control PLL as well as the location of the two samples used for the identification. Further work needs to be done to explore algorithms sensitivity issues with respect the PLL bandwidths, sampling times,

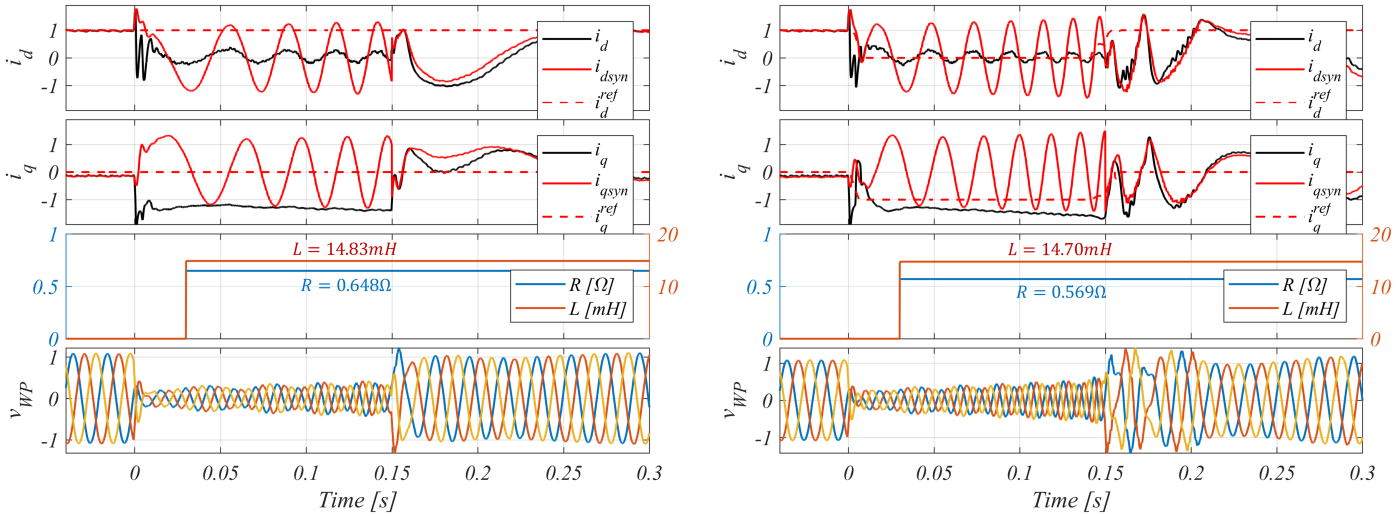

(a) Identification of grid impedance during active current injection. $\hat{R} = 0.648\Omega$ and $\hat{L} = 14.83mH$.

(b) Identification of grid impedance during current injection based on grid code. $\hat{R} = 0.569\Omega$ and $\hat{L} = 14.70mH$.

Fig. 7: Experimental verification of the detailed simulation results in Fig. 6. $\hat{\mathbf{V}}_{\mathrm{G}} = 0.05$ pu during the fault.

current references and the like. This work will inform what improvements can be made to enhance the accuracy of this method.

V. Conclusions

Under severe fault conditions the voltage at renewable energy connection points can become unstable. This is especially the case if the connection point control is injecting reactive current, as dictated by most grid codes. It is known that with knowledge of the grid fault impedance it is possible, via control, to avert this instability and satisfy the grid codes.

The key result in this paper is the development of a new rapid grid fault impedance identification algorithm, where the grid fault itself is used as the excitation pulse for the impedance identification. This algorithm eliminates the need for a user induced test pulse. Simulation studies and experimental results verify that the algorithm is able to accurately identify the grid impedance during a fault. If the grid fault impedance is known, then control strategies can be developed to prevent renewable connection point instability.

Future work will consider the effects that the sampling interval and PLL bandwidth has on the accuracy of the algorithm.

References

[1] D. Dong, J. Li, D. Boroyevich, P. Mattavelli, I. Cvetkovic, and Y. Xue, "Frequency behavior and its stability of grid-interface converter in distributed generation systems," in *2012 Twenty-Seventh Annual IEEE Applied Power Electronics Conference and Exposition (APEC)*, pp. 1887–1893, Feb 2012.

[2] D. Dong, B. Wen, D. Boroyevich, P. Mattavelli, and Y. Xue, "Analysis of phase-locked loop low-frequency stability in three-phase grid-connected power converters considering impedance interactions," *IEEE Transactions on Industrial Electronics*, vol. 62, pp. 310–321, Jan 2015.

[3] Ö. Göksu, R. Teodorescu, C. L. Bak, F. Iov, and P. C. Kjær, "Instability of wind turbine converters during current injection to low voltage grid faults and pll frequency based stability solution," *IEEE Transactions on Power Systems*, vol. 29, pp. 1683–1691, July 2014.

[4] J. Steinkohl, M. G. Taul, X. Wang, F. Blaabjerg, and J. Hasler, "A synchronization method for grid converters with enhanced small-signal and transient dynamics," in *2018 IEEE 19th Workshop on Control and Modeling for Power Electronics (COMPEL)*, pp. 1–7, June 2018.

[5] M. G. Taul, X. Wang, P. Davari, and F. Blaabjerg, "Grid synchronization of wind turbines during severe symmetrical faults with phase jumps," in *IEEE ECCE*, (Portland Oregon), Institute of Electrical and Electronic Engineers, Oct 2018.

[6] M. G. Taul, X. Wang, P. Davari, and F. Blaabjerg, "An overview of assessment methods for synchronization stability of grid-connected converters under severe symmetrical grid faults," *IEEE Trans. Power Electron.*, pp. 1–1, 2019.

[7] I. Erlich, F. Shewarega, S. Engelhardt, J. Kretschmann, J. Fortmann, and F. Koch, "Effect of wind turbine output current during faults on grid voltage and the transient stability of wind parks," in *2009 IEEE Power Energy Society General Meeting*, pp. 1–8, July 2009.

[8] H. Gu, X. Guo, D. Wang, and W. Wu, "Real-time grid impedance estimation technique for grid-connected power converters," in *2012 IEEE International Symposium on Industrial Electronics*, pp. 1621–1626, May 2012.

[9] N. Hoffmann and F. W. Fuchs, "Online grid impedance estimation for the control of grid connected converters in inductive-resistive distributed power-networks using extended kalman-filter," in *2012 IEEE Energy Conversion Congress and Exposition (ECCE)*, pp. 922–929, Sept 2012.

[10] J. Hui, H. Yang, S. Lin, and M. Ye, "Assessing utility harmonic impedance based on the covariance characteristic of random vectors," *IEEE Transactions on Power Delivery*, vol. 25, pp. 1778–1786, July 2010.

[11] D. Borkowski and S. Barczentewicz, "Power grid impedance tracking with uncertainty estimation using two stage weighted least squares," *Metrology and Measurement Systems*, vol. XXI, no. 1, pp. 99–110, 2014.